Self-diffusivity and interdiffusivity of molten aluminum-copper alloys under pressure, derived from molecular dynamics

Robert E. Rudd, William H. Cabot, Kyle J. Caspersen, Jeffrey A. Greenough, David F. Richards, Frederick H. Streitz, and Paul L. Miller

Phys. Rev. E **85**, 031202 — Published 27 March 2012

DOI: 10.1103/PhysRevE.85.031202

Self-Diffusivity and Interdiffusivity of Molten Aluminum-Copper Alloys under Pressure, Derived from Molecular Dynamics

Robert E. Rudd,* William H. Cabot, Kyle J. Caspersen, Jeffrey A. Greenough, David F. Richards, Frederick H. Streitz, and Paul L. Miller
Lawrence Livermore National Laboratory, L-045, Livermore, California 94551 USA

We use molecular dynamics (MD) to simulate diffusion in molten aluminum-copper (AlCu) alloys. The self-diffusivities and Maxwell-Stefan diffusivities are calculated for AlCu mixtures using the Green-Kubo formulas at temperatures from 1000 K to 4000 K and pressures from 0 GPa to 25 GPa, along with some additional points at higher temperatures and pressures. The diffusivities are corrected for finite size effects. The Maxwell-Stefan diffusivity is compared to the diffusivity calculated from the self-diffusivities using a generalization of the Darken equation. We find that the effects of cross-correlation are small. Using the calculated self-diffusivities, we have assessed whether dilute hard sphere and dilute Lennard-Jones models apply to the molten mixture. Neither of the two dilute gas diffusivities describes the diffusivity in molten Al and Cu. We report generalized analytic models for the self-diffusivities and interdiffusivity (mutual diffusivity) that fit the MD results well. The MD-derived transport coefficients are in good agreement with the available experimental data. We also report MD calculations of the viscosity and an analytic fit to those results. The ionic thermal conductivity is discussed briefly.

PACS numbers: 66.10.cg, 64.75.Ef, 61.20.Ja

I. INTRODUCTION

The mixing of dissimilar fluids is important to a wide variety of natural and industrial processes. The mixing of fuel and air in combustion [1], the mixing of hormones in signaling processes in biological cells [2], and the mixing of pollutants and other particles in the atmosphere [3] are but a few of the processes of great importance and under active study. In metallic systems there is interest in mixing in planetary interiors [4] and alloy processing [5]. Even the deuterium-tritium mixtures at the conditions for inertial fusion energy are dense metallic fluids and mixing affects the threshold for ignition [6]. Mixing generally involves stirring and diffusion. Stirring results from the advective flow of one fluid into another due to conservation of momentum and the forces imparted to the fluids; diffusion is the interpenetration of the fluids at the atomic level as the system seeks to lower its chemical potential through a random walk of the atoms that tends to reduce concentration gradients.

In this Article we mainly consider diffusion in molten aluminum-copper alloys. We use the aluminum-copper system as an example of transport in molten metal mixtures at high temperature and high pressure, examining how the diffusivity changes with compression, temperature and concentration. There are several reasons why diffusion in the molten aluminum-copper system is interesting. It combines the challenges of dense fluids, fluid mixtures, molten metals and material-specific properties. While diffusion in dilute gases has been studied extensively and is well understood in many respects [7], the theory of diffusion in dense fluids is not as advanced; in particular, the analytic models of diffusion in dense fluids are typically limited to relatively narrow ranges of thermodynamic conditions such as along the melt curve. Molten aluminum and copper comprise a dense system with each atom in constant interaction with its neighbors through metallic bonds. The properties of the aluminum and copper atoms in the mixture are not trivial. Aluminum and copper have atomic volumes that differ at ambient pressure, with the volume of aluminum about 50% greater than that of copper. The two are completely miscible as liquids [8], whereas the solid binary alloys show a remarkably complex phase diagram due in part to the volume mismatch. Some of these phases are very important for industry because copper-rich phases precipitate and strengthen aluminum alloys. The molten alloys we study show no tendency to phase segregate or form molecules. There is a weak but non-negligible chemistry as the internal energy for the mixed state is slightly preferable to the phase separated state, with the mixed state further promoted by the entropy of mixing. Some experimental measurements of transport properties have been made for these metals [9–18]. This combination of properties makes the molten aluminum-copper system interesting as an archetype for transport properties in dense fluids, especially molten metal alloys.

*Electronic address: robert.rudd@llnl.gov

We have used the aluminum-copper system to study atomic scale effects in hydrodynamic flows [19], such as in the Kelvin-Helmholtz instability in which ripples grow on the interface between two fluids flowing past each other [20]. As the instability enters the non-linear regime, the ripples transition to well-defined vortices that continue to grow in size. The billows (commonly known as waves) that form on the top of water as air blows across it are a familiar example of a manifestation of such a shear instability. In a shear layer the vortices that form stir the fluids, moving one fluid into the other through advection. Diffusion further promotes the mixing. The simulations of the Kelvin-Helmholtz instability at the atomic scale using molecular dynamics (MD) were extremely expensive in terms of computational resources. A specific motivation of the work presented here is to construct a model of the diffusive part of the mixing for use in continuum fluid instability simulations and analysis of the large MD simulations.

Diffusivity in fluid mixtures is not well understood except in certain limits. In particular, only in these limits are models available that describe the diffusivity across a broad range of temperatures and pressures. In the dilute gas limit, diffusion involves long ballistic trajectories with occasional binary collisions. Diffusivities can be calculated analytically in terms of scattering integrals using Chapman-Enskog theory. The expressions for self-diffusivities due to Chapman and Cowling are well known [7, 21, 22]. In the other extreme, diffusion in solids involves long oscillations in the potential well associated with one lattice site punctuated by rare events in which the diffusing species hops to another well before continuing its oscillations there [23]. That process is typically described by transition state theory [24], and a theory has been developed that relates the diffusivity to excess entropy [25, 26]. Dense fluids are between the dilute gas and solid limits. Diffusion of molecules in the fluid is impeded by a cage of surrounding molecules, and there is a time scale associated with the persistence of that cage that controls diffusion [27–29].

Diffusion has been studied in experiments involving a variety of molten metals [30], often over a small range of temperatures at ambient or near-ambient pressure or near the solidification curve (liquidus) under pressure. The use of inelastic scattering to infer dynamic correlation functions, and hence the diffusivity, has proved very valuable. Hard sphere numerical studies using molecular dynamics [31] and Monte Carlo [32] approaches have been used as standard reference systems to infer the equation of state and transport behavior of fluids under these conditions [30, 33, 34]. Such reference systems have proved to be very valuable in understanding the fluid behavior in the relatively narrow range of conditions near the solidification curve. More realistic interatomic potentials have also been used in MD to study diffusion at low pressure [35–40]. Mode coupling theory [41] has provided a sophisticated statistical mechanics framework to understand diffusivity experiments, and especially glassy systems. In all of this work there is no theoretical prediction for the diffusivity of dense fluids that has been tested over a broad range of temperature, pressure and concentration.

Here we use molecular dynamics [31, 42] with forces derived from classical interatomic potentials to simulate diffusion in homogeneous molten aluminum-copper (AlCu) alloys. To the best of our knowledge, this work is the first study to use MD with material-specific interactions to quantify diffusion processes in dense fluid mixtures across a broad range of conditions. Prior classical and quantum MD simulations with material-specific forces have been used to calculate diffusivities at specific thermodynamic conditions [43–45]. The terms classical and quantum here and throughout the Article refer to how the forces are computed, either from a classical potential or from explicitly solving quantum-mechanical equations for the electrons (in both, the ions typically are evolved according to classical equations of motion). The self-diffusivities (tracer diffusivities) and Maxwell-Stefan diffusivities are calculated using fluctuation-dissipation relations (Green-Kubo formulas). Here we use that approach for the molten alloy at various copper fractions. These calculations concentrate on a range of temperatures from 1000 K to 4000 K and pressures from 0 GPa to 25 GPa, with some additional calculations at higher temperatures and pressures. This represents a significant pressure range and temperatures that are not restricted to near the solidification curve. The Maxwell-Stefan diffusivities are used to estimate the interdiffusivity (also termed the Fickian diffusivity and the mutual diffusivity), which is compared to that predicted by a generalization of the Darken equation. Analytic models of the self-diffusivity and interdiffusivity are constructed. Also, the viscosity and thermal conductivity are discussed.

II. CONTINUUM FLUID MECHANICS

Species diffusion in response to concentration gradients is one contribution to how fluids evolve in time. They also respond to pressure gradients, thermal gradients, forces and boundaries in a way that respects conservation of mass, momentum, and energy, and well as conserving numbers of atoms (perhaps evolving the species populations according to the kinetic laws associated with chemistry and/or nuclear transformations). In the AlCu system, nuclear transformations and chemical reactions leading to changes in molecular populations are not important.

The details of the way in which the full set of equations of fluid mechanics are formulated determine the diffusion equations and the diffusivity. To show that dependence we consider the equations here. The conservation laws and dissipative fluxes are described by the Navier-Stokes Equations for multicomponent fluids. The complete set of these equations is complicated and given in standard texts (for example, see Bird, Stewart and Lightfoot, Ref. 7, Ch. 19).

Here we consider the binary fluid case, and only write the equations that are relevant to diffusion. The conservation equations for mass and momentum and the equation for the species flux (neglecting body forces other than gravity) are:

$$\frac{D\rho}{Dt} = -\rho\,\nabla\cdot\mathbf{v} \tag{1}$$

$$\rho\,\frac{D\omega}{Dt} = -\nabla\cdot\mathbf{j} + r \tag{2}$$

$$\rho\,\frac{D\mathbf{v}}{Dt} = -\nabla p - [\nabla\cdot\tau] + \rho\mathbf{g} \tag{3}$$

$$\mathbf{j} = -\rho\mathscr{D}_{12}\left[\nabla\omega + (k_T/T)\nabla T + (k_p/p)\nabla p\right] \tag{4}$$

where Df/Dt is the comoving derivative (e.g. $D\rho/Dt = \partial_t\rho + \mathbf{v}\cdot\nabla\rho$). $\mathbf{v}(\mathbf{x})$ is the velocity field, $\rho(\mathbf{x})$ is the density, $\mathbf{g}$ is the gravitational acceleration, $\omega(\mathbf{x})$ is the mass fraction of one species (here taken to be copper), $\mathscr{D}_{12}$ is the interdiffusivity (the transport coefficient for Fickian species diffusion), k_T is the thermal diffusion ratio, $k_P\mathscr{D}_{12}$ is the barodiffusion coefficient, $k_T\mathscr{D}_{12}$ is the thermal diffusion coefficient. The rate of production of mass of one species due to chemical reactions is r, which we will take to be zero. The equations are written in the form suitable for binary mixtures. For higher order mixtures, the mass fraction, mole fraction, reaction rate, flux and associated transport coefficients are species-dependent and carry an additional index that we have suppressed. The equation of state is a specified function $p(\rho, T, \omega)$.

τ_{ij} is the energy-momentum tensor (related to the stress tensor σ_{ij} by $\tau_{ij} = \rho v_i v_j - \sigma_{ij}$). The other fields are the internal energy per unit mass, E, the pressure $p = -\frac{1}{3}\sigma_{ii}$, and the temperature T. In Newtonian fluids the viscous stress tensor is given by

$$\sigma'_{ij} = \eta\left(\partial_i v_j + \partial_j v_i - \frac{2}{3}\delta_{ij}\partial_k v_k\right) + \zeta\delta_{ij}\partial_k v_k \tag{5}$$

where η is the shear viscosity, and ζ is the bulk viscosity. The full stress tensor is related to the viscous part by $\sigma_{ij} = -p\delta_{ij} + \sigma'_{ij}$. A suitable set of boundary and initial conditions is also needed to fully specify a flow.

We are principally interested in Fick's Law, which is implied by Eqs. (2) and (4) and corresponds to the case where there is no density variation, no temperature gradient and no stress:

$$0 = \partial_t(\omega\rho) + \nabla\cdot(\omega\rho\mathbf{v} + \mathbf{j}) \tag{6}$$

$$\mathbf{j} = -\rho\mathscr{D}_{12}\nabla\omega \tag{7}$$

For some generality, we have retained the velocity $\mathbf{v}$.

III. TRANSPORT COEFFICIENTS

A. Self-diffusivity, viscosity and thermal conductivity

There are three transport coefficients of fluids that have been studied extensively and may be formulated as the integral of certain time autocorrelation functions suitable for calculation in molecular dynamics (MD) using the Green-Kubo formalism [34, 45–47]: the self-diffusivity D_i, the shear viscosity η, and the thermal conductivity, λ. The Green-Kubo formulas for these coefficients involve integrals over autocorrelation functions [cf. McQuarrie [46], §21-8]:

$$D_i = \int_0^\infty dt\,\langle \dot{x}_i(0)\,\dot{x}_i(t)\rangle \tag{8}$$

$$\eta = \frac{V_{tot}}{k_{\mathrm{B}}T}\int_0^\infty dt\,\langle \sigma_{xy}(0)\,\sigma_{xy}(t)\rangle \tag{9}$$

$$\lambda = \frac{V_{tot}}{k_{\mathrm{B}}T^2}\int_0^\infty dt\,\langle J^e_x(0)\,J^e_x(t)\rangle \tag{10}$$

where the index i labels the species. By self-diffusivity we mean the diffusivity for species i in the mixture; we do not imply that the fluid is pure species i. The autocorrelation function that enters the expression for the self-diffusivity D_i only depends on the velocities of species i. Here we are following the usual convention, but we emphasize the point because the terminology can lead to some confusion. V_{tot} is the total volume of the simulation, k_{B} is the Boltzmann

constant, T is the absolute temperature, $\dot{x}(t)$ is the velocity in the x direction, $\sigma_{ij}(t)$ is the (virial) stress and $J_x^e(t)$ is the energy current:

$$\sigma_{ij} = -\frac{1}{V_{tot}}\left(\sum_\mu m_\mu \dot{x}_{\mu i}\dot{x}_{\mu j} + \sum_{\langle\mu\nu\rangle} x_{\mu\nu i}F_{\mu\nu j}\right) \tag{11}$$

$$J_i^e = \frac{1}{V_{tot}}\left[\sum_\mu \dot{x}_{\mu i}\left(e_\mu - \langle h\rangle\right) + \sum_{\langle\mu\nu\rangle} x_{\mu\nu i}\left(\frac{\dot{x}_\mu + \dot{x}_\nu}{2}\right)\cdot F_{\mu\nu}\right] \tag{12}$$

$$e_\mu = \frac{1}{2}m_\mu\left|\dot{x}_\mu\right|^2 + U_\mu \tag{13}$$

$$\langle h\rangle = \left(\frac{1}{N}\sum_\mu e_\mu\right) + p\,V \tag{14}$$

where μ and ν label atoms and the sums over $\langle\mu\nu\rangle$ sum distinct pairs of atoms. The relative separation is $x_{\mu\nu i} = x_{\mu i} - x_{\nu i}$. m_μ is the mass of atom μ and U_μ is its potential energy. In practice these formulas converge more rapidly if averaged over the different independent components of velocity, stress and current.

The Green-Kubo formula for self-diffusivity (8) involves an integral over the velocity autocorrelation function

$$Z_i(t) = \langle\dot{x}_i(t)\dot{x}_i(0)\rangle \tag{15}$$

$$= \frac{1}{3}\langle\dot{\mathbf{x}}_i(t)\cdot\dot{\mathbf{x}}_i(0)\rangle \tag{16}$$

This autocorrelation depends on the species i, as well as the pressure, temperature and copper fraction. The autocorrelation function starts with a value of $Z_i(0) = k_\mathrm{B}T/m_i$ and decreases to zero as time progresses, perhaps with some oscillations. The Green-Kubo expression for the self-diffusivity in a homogeneous system is equivalent to the definition:

$$D_i = \lim_{t\to\infty}\frac{1}{6t}\langle\left|\mathbf{x}_i(t) - \mathbf{x}_i(0)\right|^2\rangle, \tag{17}$$

The Green-Kubo expression can be recovered by replacing $\mathbf{x}$ in this expression with the time integral of the velocity (cf. Ref. 34, Section 7.2).

B. Interdiffusion

The interdiffusivity is also of interest, and it requires a different Kubo formula. Interdiffusion is the process described by Fick's equation (2). It moves one species with respect to the others. For example, it controls the rate of broadening of the interface between regions of different concentration. As such, it can be calculated directly with non-equilibrium molecular dynamics. We return to this point below. It can also be calculated using linear response theory and fluctuation-dissipation relations, similar to how the self-diffusivity is calculated.

The interdiffusion current involves the relative transport of mass. In a binary system the mass flow of one component relative to the other is given by (cf. Refs. [7, 34]):

$$\mathbf{j}^c = \rho_1\mathbf{v}_1 - \rho_2\mathbf{v}_2 \tag{18}$$

$$= \rho_1\rho_2\left(\mathbf{v}_1 - \mathbf{v}_2\right)/\rho + \left(\rho_1 - \rho_2\right)\mathbf{v} \tag{19}$$

$$= \omega_1\omega_2\,\rho\,\left(\mathbf{v}_1 - \mathbf{v}_2\right) \tag{20}$$

where ρ_i and $\mathbf{v}_i$ are the mass density and the center-of-mass velocity of species i. The third expression is valid in the center-of-mass frame ($\mathbf{v} = 0$). Often the interdiffusivity is written as a number flux instead of the mass flux given here, and in that case the flux is the same up to a mass-dependent constant [34]: $X_1X_2\,n\,\left(\mathbf{v}_1 - \mathbf{v}_2\right)$ where n is the number density.

The relation between interdiffusivity and self-diffusivity may be presented in terms of Maxwell-Stefan diffusivity. For a binary mixture, the Maxwell-Stefan equations take the form [7]:

$$\frac{X_1 X_2 \left(\mathbf{v}_1 - \mathbf{v}_2\right)}{Đ_{12}} = \frac{X_1}{k_B T} \nabla \mu_1 \tag{21}$$

where $\mathbf{v}_i$ is the mean velocity of species i and μ_i is the chemical potential of species i. $Đ_{12}$ is the Maxwell-Stefan diffusivity, which is related to, but not equal to, the interdiffusivity. Rearranging Eq. (21), reexpressing the velocity difference in terms of the mass flux, and using the chain rule for the gradient we have

$$\begin{aligned} \mathbf{j}^c &= \rho\, Đ_{12} \frac{m_1 m_2}{X_1 m_1 + X_2 m_2} \frac{X_1}{k_B T} \frac{\partial \mu_1}{\partial X_1} \nabla X_1 & (22) \\ &= \rho\, Đ_{12} \frac{X_1}{k_B T} \frac{\partial \mu_1}{\partial X_1} \nabla \omega_1 & (23) \end{aligned}$$

where m_i denotes the species mass. Comparison of this equation with the continuum fluid equations (7) shows the interdiffusivity to be:

$$\begin{aligned} \mathscr{D}_{12} &= Đ_{12} \Phi & (24) \\ \Phi &= \frac{X_1}{k_B T} \frac{\partial \mu_1}{\partial X_1} & (25) \end{aligned}$$

Here Φ is called the thermodynamic factor [45]. It can be expressed in terms of the activity as

$$\Phi = 1 + \frac{d \log f_1}{d \log X_1} \tag{26}$$

where f_i is the activity coefficient of species i [51]. The activity vanishes for ideal fluid mixtures, so the thermodynamic factor is equal to unity in that case.

The expression for the Maxwell-Stefan binary diffusivity may be derived from linear response theory, and it involves the autocorrelation function of the interdiffusion current (18): $Đ_{12} \propto \int_0^\infty dt \, \langle \mathbf{j}^c(0) \cdot \mathbf{j}^c(t) \rangle$ [48–50]:

$$\begin{aligned} Đ_{12} &= \int_0^\infty dt \, Z_{\mathrm{MS}}(t) & (27) \\ Z_{\mathrm{MS}}(t) &= \frac{X_1 X_2 N}{3} \langle [\mathbf{v}_1(0) - \mathbf{v}_2(0)] \cdot [\mathbf{v}_1(t) - \mathbf{v}_2(t)] \rangle & (28) \end{aligned}$$

where N is the total number of atoms.

C. Relating Self-Diffusion to Interdiffusion

The Maxwell-Stefan diffusivity contains cross-correlation contributions that are not contained in the self-diffusivity. It is interesting to consider whether those cross-correlation terms are important. There is an approximate expression for the interdiffusivity in terms of the self-diffusivities that was developed for diffusion in solid metals by Darken [51–54]. It is an approximate relation, but it often works well in practice [55]. The high temperature molten metals studied here are expected to be described well by this approximate relation.

A derivation of the expression [48] starts with the Maxwell-Stefan diffusivity (27) and then eliminates cross-correlations:

$$\begin{aligned} Đ_{12} &= \frac{X_1 X_2 N}{3} \int_0^\infty dt \, \langle [\mathbf{v}_1(0) - \mathbf{v}_2(0)] \cdot [\mathbf{v}_1(t) - \mathbf{v}_2(t)] \rangle \\ &= \frac{X_1 X_2 N}{3} \int_0^\infty dt \, \Big\langle \left[\frac{1}{N_1} \sum_{i \in 1} \dot{\mathbf{x}}_i(0) - \frac{1}{N_2} \sum_{j \in 2} \dot{\mathbf{x}}_j(0) \right] \\ &\qquad \cdot \left[\frac{1}{N_1} \sum_{i \in m} \dot{\mathbf{x}}_m(t) - \frac{1}{N_2} \sum_{n \in 2} \dot{\mathbf{x}}_n(t) \right] \Big\rangle & (29) \\ &\approx X_1 X_2 N \left(\frac{1}{N_1} D_1 + \frac{1}{N_2} D_2 \right) & (30) \\ &= X_2 D_1 + X_1 D_2 & (31) \end{aligned}$$

where in going from (29) to (30) it was assumed that the cross-correlations vanish: $\langle \dot{\mathbf{x}}_i(0) \cdot \dot{\mathbf{x}}_j(t) \rangle = 0$ unless $i = j$. This equation relates the Maxwell-Stefan diffusivity $Đ_{12}$ to the self-diffusivities D_i. It is a form of the Darken equation [51]. All of these transport coefficients are evaluated at the relevant conditions: $Đ_{12}(T, p, \omega)$ and $D_i(T, p, \omega)$. For AlCu interdiffusivity the Darken relation is then

$$\mathscr{D}_{12} \;=\; [(1-X)D_{\rm Cu} + X D_{\rm Al}]\,\Phi \tag{32}$$

where X is the copper mole fraction.

However, since the diffusion is taking place in the center of mass frame, the motion of different atoms is not strictly uncorrelated, even if one assumes that the motions of neighboring atoms are otherwise uncorrelated. This correlation causes some ambiguity in the derivation of the Darken relation (31). In the center-of-mass frame, the species velocities that enter the autocorrelation function for the Maxwell-Stefan diffusivity satisfy

$$\mathbf{v}(t) \;=\; \omega_1 \mathbf{v}_1(t) + \omega_2 \mathbf{v}_2(t) = 0 \tag{33}$$

so that

$$\mathbf{v}_1(t) - \mathbf{v}_2(t) \;=\; \frac{1}{\omega_2}\,\mathbf{v}_1(t). \tag{34}$$

This expression is exact in the center-of-mass frame. Using this relation, the Maxwell-Stefan diffusivity may be reexpressed as

$$Đ_{12} \;=\; \frac{X_1 X_2 N}{3\omega_2^2}\int_0^\infty dt\,\langle \mathbf{v}_1(0)\,\mathbf{v}_1(t)\rangle \tag{35}$$

$$\approx\; \frac{X_2}{\omega_2^2} D_1 \tag{36}$$

The expression (35) is exactly equal to Eq. (27), but the expression that results when the cross-correlations are neglected (36) can be quite different than the Darken expression (31). Similar manipulations keeping $\mathbf{v}_2$ rather than $\mathbf{v}_1$ leads to the approximation

$$Đ_{12} \approx (X_1/\omega_1^2) D_2. \tag{37}$$

For two unequal species masses, the approximations (31), (36) and (37) for $Đ_{12}$ can be significantly different.

This *reductio ad absurdum* leads us to consider the derivation of a similar expression starting with the diffusion equation and imposing the center-of-mass constraint. The mass currents neglecting cross-correlations are given by the following expressions in a frame moving with velocity $\mathbf{v}$ with respect to the rest frame in which the self-diffusivities are calculated:

$$\mathbf{j}_1' \;=\; -\rho D_1 \Phi \nabla\omega + \omega\rho\mathbf{v} \tag{38}$$

$$\mathbf{j}_2' \;=\; -\rho D_2 \Phi \nabla(1-\omega) + (1-\omega)\rho\mathbf{v} \tag{39}$$

where the prime is used to distinguish the individual mass currents from the total diffusive current. These equations are similar to Darken's starting point for analyzing diffusion in solids [51]. By neglecting the cross-correlations, the mass currents no longer balance, and a new center-of-mass frame must be found. The condition that the total mass flux vanish in the center-of-mass frame is given by

$$0 \;=\; \mathbf{j}_1' + \mathbf{j}_2' \tag{40}$$

$$\;=\; -\rho\,(D_1 - D_2)\,\Phi\nabla\omega + \rho\mathbf{v} \tag{41}$$

and thus

$$\mathbf{v} \;=\; (D_1 - D_2)\,\Phi\nabla\omega. \tag{42}$$

Substituting this expression for the background velocity into Eq. (38), we find the current

$$\mathbf{j} \;=\; -\rho\,[D_1 - \omega\,(D_1 - D_2)]\,\Phi\,\nabla\omega \tag{43}$$

From this equation we read off the interdiffusivity:

$$\mathscr{D}_{12} \;=\; [(1-\omega)\,D_1 + \omega D_2]\,\Phi \tag{44}$$

where for AlCu mixtures $D_1 = D_{\rm Cu}$, $D_2 = D_{\rm Al}$ and ω is the copper mass fraction. This expression is similar to the standard Darken relation (31), except that the self-diffusivities are weighted by the mass fraction rather than the mole fraction. We consider this expression below, and compare the Maxwell-Stefan diffusivity to both it and the mole-fraction-weighted (conventional) Darken relation. The change in using mass fraction weighting from mole fraction weighting can be estimated as

$$\Delta D/D \approx \frac{1}{4}\frac{\Delta m}{\bar{m}}\frac{\Delta D}{\bar{D}} \tag{45}$$

where $\Delta m = m_2 - m_1$ and $\Delta D = D_2 - D_1$ and $\bar{m}$ and $\bar{D}$ are the corresponding averages. For the AlCu system this change turns out to be $< 2\%$, so the differences are not very important. We make a quantitative comparison below.

IV. MOLECULAR DYNAMICS

We now turn to the calculation of the diffusivity as a function of copper fraction, pressure and temperature. For this purpose we have conducted molecular dynamics (MD) simulations of molten aluminum-copper (AlCu) mixtures. The simulations are in the following range of conditions: copper mole fraction X=0–1, pressure p=0–25 GPa, and temperature T=1000–4000 K, and some additional simulations at higher temperatures and pressures. MD simulates the motion of atoms interacting by forces derived from an interatomic potential. We used the FEMD code [56–58] with the Mason-Rudd-Sutton interatomic potential for AlCu alloys [59] which is in the Finnis-Sinclair family of potentials [60]. This AlCu potential has also been used to study diffusion in solid AlCu alloys [59, 61, 62], and details of how the potential was constructed are in those publications. The potentials, like other Finnis-Sinclair and Embedded Atom Method potentials, are many-body potentials, so the force experienced by an atom depends on the density due to the cluster of neighboring atoms and cannot be factorized into pairwise interactions. In this formulation properties of the solid including densities, cohesive energies and elastic constants agree with the experimental data (within the error bars on those data). This level of agreement with experiment is not possible with pair potentials (pairwise interactions).

The atoms move according to Newton's Third Law (F=ma), with the set of $3N$ coupled ordinary differential equations integrated explicitly in time using a velocity Verlet time integrator with a time step of 2 fs, reduced to 0.5 fs for simulations with $T \geq 20000$ K. The atomic configuration for the self-diffusivity and viscosity calculations consisted of N=4000 atoms, generated from a well equilibrated molten Al system with a fraction of the atoms changed at random to Cu to obtain the required mole fraction, scaling the velocity so that the kinetic energy remained the same despite the change in mass. The center-of-mass velocity was zero. The interdiffusivity calculations were done for a subset of the thermodynamic conditions with N=256000 atoms for ten million time steps ($\sim$ 20 ns), and the self-diffusivities and viscosities were calculated for these runs as well, to confirm the size scaling formulas described below. This procedure for creating the initial configuration starts with a liquid that is homogeneous at the microscopic level (up to statistical fluctuations), and thus avoids the persistent micro-heterogeneity that has been observed in some molten aluminum alloys produced by melting weakly order solid alloys and not subjected to a critical overheating beyond the liquidus [63]. The system was then re-equilibrated over $\sim$ 10 ps with a thermostat (velocity renormalization) to obtain the desired temperature and scaling the simulation box volume to obtain the desired pressure (calculated with the virial stress formula (11)). The size of the cubic simulation box was 3.6 to 4.8 nm on a side for the 4000 atom simulations (up to 16 nm for the 256000 atom simulations), depending on the thermodynamic conditions with a small number of larger simulations up to 16 nm on a side. Periodic boundary conditions were used. Following the initial gross equilibration, the system was further equilibrated at constant volume with a weak thermostat (velocity renormalization every 100 time steps) for 100 ps. Simulations were conducted at 165 combinations of mole fractions and thermodynamic conditions: $X = 0.0, 0.1, \ldots, 1.0$, $T = 1000, 2000, 3000$ K, and $p = 0, 2, 4, 10, 25$ GPa. A few additional simulations were run in pure Al and pure Cu at $T \geq 4000$ K.

Once the system was equilibrated, the simulation was run for an additional 6.4 ns, calculating the velocity autocorrelation function on the fly. Each 4000-atom run took about 10 hours on 8 CPU's on the *Zeus* supercomputer at Lawrence Livermore [64], and we conducted a total of 383 such runs, with more than one run at each set of conditions in order to improve statistics. Each 256000-atom run took about 16 hours on 64 CPU's on the *Atlas* supercomputer at Lawrence Livermore [64] for a simulated time of 1 ns. For each atom the initial velocity was saved. The autocorrelation function was calculated as the simulation progressed:

$$Z_i(t) = \frac{1}{3}\frac{1}{N_i}\sum_{\alpha\in i}\dot{\mathbf{x}}_\alpha(0)\cdot\dot{\mathbf{x}}_\alpha(t) \tag{46}$$

where i indicates the type of atom (Al or Cu) and N_i is the number of that type. The simulation was run on a parallel supercomputer, so the initial velocity was part of the information that had to be communicated if the atom

moved from the spatial domain associated with one processor to that associated with another. Since the velocity is used rather than the position, no special bookkeeping is required if an atom diffuses around the periodic boundaries. The correlation function was saved as a table with an entry per time step. After a sufficiently long period (10 ps), the autocorrelation function was zero apart from statistical noise, so a new initial velocity was saved and additional contributions to the autocorrelation function were calculated, further reducing the statistical noise. This approach is similar to earlier calculations of self-diffusivities in MD (cf. Ref. 65).

The self-diffusivity was then calculated as an integral (sum) over the velocity autocorrelation function by post-processing:

$$\begin{aligned} D_i &= \int_0^\infty dt\, Z_i(t) \\ &\approx \left[\sum_k a_k\, \Delta t\, Z_i(t_k)\right] + \frac{t_{\max}}{\alpha - 1}\, Z_i(t_{\max}) \end{aligned} \tag{47}$$

where the coefficients a_k give the Simpson's rule approximation to the integral. The integral/sum was terminated to account for a power-law $t^{-\alpha}$ decay in the correlation function following Bastea [44]. In particular, the long-time tail contribution was included through the final term in Eq. (47). It is well known that velocity autocorrelation functions exhibit long-time tails [66], where the exponent derived for hard spheres in three dimensions is $\alpha = 3/2$. In practice for our simulations at these elevated temperatures the long-time tail contribution was small (6% or less). The tails are discussed more in Section IV A.

In principle the integral for the Maxwell-Stefan diffusivity should be terminated similarly to account for the long-time tail of its kernel. In practice, the correlation function Z_{MS} is not converged as well as Z_{Al} and Z_{Cu}, and noise in the tail leads to noticeable noise in $Đ_{12}$. We find that in practice a more rapidly convergent expression for $Đ_{12}$ is

$$Đ_{12} \approx \left[\sum_k a_k\, \Delta t\, Z_{\mathrm{MS}}(t_k)\right] + \frac{t_{\max}}{\alpha - 1}\, Z_{\mathrm{D}}(t_{\max}) \tag{48}$$

where $Z_{\mathrm{D}}(t)$ is a correlation function suggested by the Darken relation that is discussed below (54).

As the size of the simulation box approaches the inter-atom separation, there are corrections to the self-diffusivity since the hydrodynamic flow of the atoms needed to accommodate the diffusion is impeded. The formula for this correction for a cubic periodic box with edges of length L is [67]

$$D_i = D_{\mathrm{PBC}} + \xi_{\mathrm{PBC}}\, k_{\mathrm{B}} T/(6\pi\eta L) \tag{49}$$

where $\xi_{\mathrm{PBC}} = 2.837297$. This formula gives the correction that must be added to the self-diffusivity calculated in a finite system with periodic boundary conditions D_{PBC} to get the actual self-diffusivity D_i. A more approximate version of the formula results from use of the Stokes-Einstein relation [34]

$$D_i = \frac{k_{\mathrm{B}} T}{2\pi\eta r_{\mathrm{gmax}}} \tag{50}$$

(slip boundary conditions) where r_{gmax} is the typical interatomic separation. This value may be taken to be the location of the first peak in the radial distribution function. Substituting it into Eq. (49), the relation becomes $D_i \approx D_{\mathrm{PBC}}/(1 - \gamma r_{\mathrm{gmax}}/L)$ where $\gamma = \xi_{\mathrm{PBC}}/3 = 0.9457657$. Since the Stokes-Einstein relation is not exact [68], the formula may be further approximated by taking $\gamma \approx 1$:

$$D_i \approx D_{\mathrm{PBC}}/(1 - r_{\mathrm{gmax}}/L) \tag{51}$$

which is good for quick estimates of the finite-size correction. For the AlCu system, the constant in the denominator of the Stokes-Einstein relation (50) is about 2.1 rather than 2, but that is a small correction to a small correction, and Eq. (51) is a good approximation for many purposes. We have verified the finite size correction formula (49) by comparing the results of the 4000 atom and 256000 atom simulations.

It should be noted that we are taking an approach based on classical MD using an available AlCu interatomic potential. Quantum molecular dynamics could be used to verify the accuracy of the classical potential, or even to calculate a few diffusivities directly. It is beyond the capabilities of existing computers to repeat these calculations exactly with quantum MD, but it might be possible in the future.

A. MD Self-Diffusivity Results

We have used MD to calculate the velocity autocorrelation functions and self-diffusivities across a broad range of conditions. Velocity autocorrelation functions are shown in Figs. 1 and 2 for aluminum. Figure 1 shows the autocorrelation function $Z_{\rm Al}(t)$ at various volumes per atom (Ω) at $T = 2000$ K (solid curves) and $T = 20000$ K (dashed curves). The curves at the lower temperature and the lower volumes show more structure (oscillations) due to correlated motion in the cage of neighbors. That structure is absent from the curves for the 20000 K simulations at volumes of 18 Å^3 per atom and greater for aluminum. Figure 2 shows $Z_{\rm Al}(t)$ at $\Omega = 18$Å^3 for a range of temperatures from 2000 K to 10000 K. Again the structure at lower temperatures is absent at the higher temperatures, with no minimum in the correlation function at $t < 0.1$ ps for temperatures above ∼10000 K. The autocorrelation functions are well converged. The statistical error in the self-diffusivity is less than 0.1% as determined from the standard deviation of the self-diffusivity calculated from subsets of the data compared to the reported value. The long-time tails are visible in the plot in Fig. 3, even at the elevated temperature of 20000 K. The tails are stronger at lower temperature, but the structure in the correlation function persists to later times so the scaling is less clear. For our simulations, we find the power-law scaling $t^{-\alpha}$ varies from the hard-sphere exponent of $\alpha = 3/2$ up to $\alpha \sim 2$ at higher pressures, and the expression for the diffusivity is terminated accordingly.

The full set of self-diffusivities is shown in Figs. 4 and 5. The first figure shows the self-diffusivities at zero pressure as a function of the copper fraction. The values fall in bands increasing with temperature at 1000 K, 2000 K and 3000 K (and one result at 4000 K). The second figure shows the self-diffusivities at 3000 K as a function of the copper fraction. In this case the bands correspond to different pressures, with the self-diffusivity decrease with increasing pressure at 0, 2, 4, 10 and 25 GPa. All of the self-diffusivities are in the molten alloys; some of the 1000 K results are in super-cooled conditions. These calculations do not have concentration gradients apart from local fluctuations, so the numbers represent tracer diffusivities. They do not include activity contributions.

In a few cases the tracer diffusivities of the pure metals have been measured at the melting temperature. For copper, the self-diffusivity was found to be 3.97×10^{-8} m^2/s in Ref. [9, 11]; our value of 3.32×10^{-8} m^2/s is about 16% lower than the experimental value. This is good agreement, especially since we have not tuned the interatomic potential to the properties of the molten metal. We are not aware of any high-pressure diffusivity experiments for copper or any diffusivity experiments for aluminum. For Al there are some theoretical works to which we can compare. Our Al self-diffusivity value at a temperature of 1000 K, 8.89×10^{-8} m^2/s, is 3% lower than the value of 9.2×10^{-8} m^2/s reported in Ref. [69] at a temperature of 1025 K, is 31% higher than the value of 6.8×10^{-8} m^2/s reported in Ref. [37] at a temperature of 1000 K and experimental density, and is 71% higher than the value of 5.19×10^{-8} m^2/s reported in Ref. [40] at a temperature of 973 K. Our result at 1000 K is in reasonable agreement with the other theoretical results, with an admittedly large scatter.

The general trend is for the self-diffusivities to increase with temperature and to decrease with pressure as expected. The diffusivities are higher for the more aluminum-rich alloys, increasing convexly upward as the aluminum content is increased. The number density of the aluminum is lower than that of copper at a given pressure, as seen already in the zero temperature lattice constants ($a_{\rm Cu} = 3.61$Å vs. $a_{\rm Al} = 4.05$Å). So the diffusivities are higher in the material with the lower number density, as is reasonable. Similarly, the Al self-diffusivities in all of the alloys are higher than the corresponding Cu self-diffusivities. The self-diffusivities of the different species do not converge at the end points ($X = 0$ and $X = 1$), so in the dilute limits the impurity diffusion is not fully coupled to the majority particles. In mixed systems, the self-diffusivities are not just linear interpolation in either mass fraction or mole fraction of the values at the end points, and furthermore the curvature is asymmetric. These properties affect the form of the fitting functions we use below.

B. MD PBC Correction Results

We have also calculated the radial distribution function $g(r)$ needed to determine the correction due to finite size effects for a simulation box with periodic boundary conditions (PBC). The radial distribution function was calculated at 1 ps intervals during a total simulation time of 2 ns for pure Al and pure Cu at pressures of 0, 2, 4, 10 and 25 GPa and temperatures of 2000 K and 3000 K. The results for Cu at 3000 K are shown in Fig. 7 with no smoothing. The results Al and for both at 2000 K follow the same trends.

The first peak in the radial distribution function $g(r)$ was used to calculate the nearest neighbor separation a needed for the finite-size correction (51). The results are shown in Table I. One interesting feature is that the value of a decreases as the temperature is increased from 2000 K to 3000 K, even though the overall box size increases due to thermal expansion. The value of a at the peak decreases even though the mid-point of the peak increases due to the anharmonicity of the interatomic forces. Using the values of a in Table I, we find that the corrections to the self-diffusivity cause an increase by a small amount, ∼6%, as shown in Fig. 8 for 4000 atoms. The correction is less

than 2% for the 256000 atom calculations. This correction is small and may be neglected for many purposes. We will not use it to modify the self-diffusivity values that are reported. However, in some cases it may be useful to account for this correction. For 4000 atoms, the expression

$$D_i/D_i^{\mathrm{PBC}} \approx 1 + \tilde{d}_1 - \tilde{d}_2\,\Omega\,(T/T_0)^{\beta} \tag{52}$$

describes the correction to an accuracy of 0.2% for pressures from 0 to 25 GPa with the parameters $\tilde{d}_1(Al) = 0.075$, $\tilde{d}_1(Cu) = 0.078$, $\tilde{d}_2(Al) = 6.31 \times 10^{-4}\text{Å}^{-3}$, $\tilde{d}_2(Cu) = 9.92 \times 10^{-4}\text{Å}^{-3}$, $\beta(Al) = 1/4$, $\beta(Cu) = 1/6$, and T_0 is a reference temperature taken to be 2000 K. Ω is the atomic volume in Å^3. For $N \neq 4000$, the coefficients $\tilde{d}_i$ are scaled by $(N/4000)^{-1/3}$. The tildes are used on the coefficients here to distinguish them from other coefficients discussed later in the paper. We have not calculated the correction for AlCu mixtures, and the hydrodynamic correction formula (49) may not apply to mixtures, but since the correction is small, linear interpolation by mole fraction should be a good approximation.

C. MD Maxwell-Stefan Diffusivity Results

We have also used MD to calculate the center-of-mass velocity autocorrelation functions and Maxwell-Stefan diffusivities across a broad range of conditions. The center-of-mass velocity autocorrelation function for the Maxwell-Stefan diffusivity converges much more slowly than the velocity autocorrelation function for the self-diffusivities. There is only one center-of-mass mode for each species, whereas there are many atoms. This leads to much better statistics for the self-diffusivities. In a typical calculation the error for the self-diffusivities is less than 0.1%, whereas for the Maxwell-Stefan diffusivity it is 3-6%. Longer runs were used to converge the results presented in this section (256000 atom simulations for 16 ns), bringing the error down to $\sim 1\%$ or less. Examples of the center-of-mass velocity autocorrelation function $Z_{\mathrm{MS}}(t)$ with mole fraction $X = 0.5$ are shown in Fig. 9. The corresponding atomic velocity autocorrelation functions $Z_i(t)$ are also shown. These examples were chosen to show the differences between the correlations functions at low temperature and high pressure, shown here at $T = 2000$ K and $p = 25$ GPa, and those at higher temperatures and lower pressures, shown here at $T = 3000$ K and $p = 0$ GPa. As the temperature increases or the pressure decreases to move away from the melt curve, the structure becomes less pronounced. The first minimum in the curve disappears. Since the starting value $Z_i(0)$ is proportional to the temperature, the initial peak is higher at higher temperatures. The width in time of the initial peak increases as the temperature increases or the pressure decreases. These trends apply to $Z_{\mathrm{MS}}(t)$ as well as the atomic velocity autocorrelation functions. The shape and structure of $Z_{\mathrm{MS}}(t)$ tends to be intermediate between $Z_{\mathrm{Al}}(t)$ and $Z_{\mathrm{Cu}}(t)$, although there are some differences, as has been observed in previous studies [49]. At the point at which the $Z_{\mathrm{Al}}(t)$ and $Z_{\mathrm{Cu}}(t)$ curves cross, $Z_{\mathrm{MS}}(t)$ is close, albeit not equal, in value.

As the concentration is varied, the Maxwell-Stefan kernel $Z_{\mathrm{MS}}(t)$ varies from nearly equal to $Z_{\mathrm{Cu}}(t)$ for Al-rich mixtures (low X) to nearly equal to $Z_{\mathrm{Al}}(t)$ in Cu-rich mixtures (high X), as shown in Fig. 10. This variation is in agreement with the guidance from the Darken equation (31), which would suggest the following relation:

$$Z_{\mathrm{MS}}(t) \;\approx\; Z_{\mathrm{D}}(t) \tag{53}$$

$$Z_{\mathrm{D}}(t) \;=\; (1-X)\,Z_{\mathrm{Cu}}(t) + X\,Z_{\mathrm{Al}}(t) \tag{54}$$

The error in this approximation, quantified as $|Z_{\mathrm{MS}}(t) - Z_{\mathrm{D}}(t)]|/Z_{\mathrm{MS}}(0)$, is found to be less than 3% at all times for AlCu at the conditions studied here. This error measure does not guarantee anything about how well the Maxwell-Stefan diffusivity is approximated by the Darken relation, and we find below that the agreement is somewhat worse than this.

A comparison of the Maxwell-Stefan diffusivity $Đ_{12}$ and the corresponding diffusivities derived from the Darken relations based on mole fraction weighting (31) and mass fraction weighting (44) of the self-diffusivities is shown in Fig. 11. Both the Darken expressions over-estimate $Đ_{12}$ by 1–15%, so by this measure the cross-correlations reduce $Đ_{12}$. In the majority of cases there is little difference between the mole fraction weighting and the mass fraction weighting; i.e., the magnitude of the cross-correlation effect considerably exceeds the difference between mass- and mole-fraction weighting. In those cases where there is a difference, the mass fraction weighting gives a result that is closer to $Đ_{12}$ (such as at $p = 0$ and $T = 3000$ K).

V. ANALYTIC DIFFUSIVITIES

We next convert the results of the self-diffusivity calculations into an analytic form suitable for continuum Navier-Stokes simulations. In the process, we compare with functional forms presented in the literature. The question of

how the diffusivity changes with pressure has been addressed in the context of gases [21] and solids [70], but there has been little work on high pressure molten metals. We will consider whether existing forms continue to apply in this different regime. In particular we consider a form that arises in the dilute gas limit from Chapman-Enskog theory [21] and a form that arises from the analysis of dense hard sphere systems mechanics [46]. We also give an empirical fit motivated by the hard sphere model.

A. Dilute Gas

We first assess whether the formula for diffusivity for dilute gases due to Chapman and Cowling [21] provides a good description of the MD-based values. Diffusion in dilute binary gas mixtures has been studied extensively [7], with the general trend that the self-diffusivity decreases with increasing pressure and increases with increasing temperature. It is not a strong function of the composition. The molten AlCu system we study is in the dense fluid regime. The atoms interact via a short-ranged potential, but even at the lowest densities studied here there are over a dozen atoms within the interaction cutoff. As a result, the atoms are in constant interaction with their neighbors, and the diffusive process is very different than ballistic trajectories with occasional binary collisions. It may be expected that the dilute-gas formula will disagree with the MD results for the molten AlCu mixtures, but the magnitude of the difference is not known *a priori*. The agreement may be good enough. For this reason, we first consider dilute gas models.

We consider the expressions for the diffusivity of a dilute gas for two cases: hard sphere and Lennard-Jones atoms. We focus on pure aluminum for the initial assessment of whether this approach is sufficiently accurate. The self-diffusivity (tracer diffusivity) of a dilute gas of hard spheres is given by [7]

$$D_{AA^*} = \beta \frac{\sqrt{m\, k_{\mathrm{B}} T}}{\rho\, d^2} \quad \text{dilute hard sphere} \tag{55}$$

where d is the hard sphere diameter and m is the mass. The prefactor is given by $\beta = 2/(3\pi^{3/2})$. Here we have made use of the ideal gas law to eliminate the pressure. If instead a dilute gas of Lennard-Jones atoms is considered, the self-diffusivity (tracer diffusivity) is

$$D_{AA^*} = \beta \frac{\sqrt{m\, k_{\mathrm{B}} T}}{\rho\, \sigma^2 \Omega_{D,AA^*}} \quad \text{dilute Lennard}-\text{Jones} \tag{56}$$

where σ is the Lennard-Jones radius (a species-dependent constant) and Ω_{D,AA^*} is the scattering integral (a function of temperature and species). The prefactor is given by $\beta = 3/(8\sqrt{\pi})$. The temperature dependence of Ω_{D,AA^*} gives the Lennard-Jones self-diffusivity an overall scaling of $D_{AA^*} \propto T^2$ at low temperatures and $D_{AA^*} \propto T^{1.65}$ at high temperatures [7].

These forms do not provide a good description of the MD diffusivities. The dilute hard sphere result for pure Al is shown in Fig. 12 with a hard sphere diameter of 2.4Å. The temperature dependence of the dilute Lennard-Jones diffusivity is too strong; that of the dilute hard sphere diffusivity is too weak. In both cases the scaling with atomic volume is linear, whereas the MD diffusivities have an affine variation (varying like a line with a non-zero intercept). We must turn to other models.

B. Hard Sphere Liquid Model

Dense hard-sphere systems have been studied extensively and have been used as a reference system for transport properties, equation of state and other thermodynamic properties. The system consists of particles that do not interact except for elastic collisions that occur when the centers of two of the particles are separated by twice the hard sphere radius. Denoting the hard sphere radius by σ, the system is characterized by the packing fraction $\xi = \frac{1}{6}\pi\sigma^3/\Omega$ where Ω is the atomic volume. The hard-sphere equation of state calculated by Alder and Wainwright [31] using molecular dynamics is well described by the analytic form due to Carnahan and Starling [33]

$$\frac{p_H \Omega}{k_{\mathrm{B}} T} = \frac{1 + \xi + \xi^2 - \xi^3}{(1-\xi)^3}. \tag{57}$$

The diffusivity of this system is given by [30, 71]

$$D_H = \frac{1}{48} \left(\frac{\pi k_{\mathrm{B}} T}{M} \right)^{1/2} \left(\frac{6\Omega}{\pi \xi^2} \right)^{1/3} \frac{(1-\xi)^3}{\xi(1-\xi/2)} \tag{58}$$

The naive hard-sphere equation of state does not describe our AlCu system well, due to the attractive forces between the atoms. This effect can be addressed by adding a uniform, volume-dependent negative background potential [30, 72], shifting the pressure:

$$p_H = p + f(\Omega). \tag{59}$$

There have been various suggestions of simple forms for this correction [30, 73]. We tried various simple forms for $f(\Omega)$ that involved sums of terms that go like inverse fractional powers of Ω, but the agreement with the MD results was poor. Another generalization of the hard-sphere form was suggested by Dymond [22], but this form also does not agree well with our MD results.

To go beyond the simple forms we note that the hard sphere system solidifies at a packing fraction of $\xi_c = 0.46$, so we can use $f(\Omega)$ to enforce $\xi = \xi_c$ on the Lindemann melt curve. Specifically, using a Grüneisen form for the equation of state with the cold pressure $p(T = 0\ K) = p_0(\Omega)$ [74], the expression for $f(\Omega)$ is

$$f(\Omega) = -p_0(\Omega) + \frac{1}{\Omega}\left(\phi(\xi_c) - 3\gamma_0/\eta\right) k_{\rm B} T_m \tag{60}$$

where $\phi(\xi) = (1 + \xi + \xi^2 - \xi^3)/(1 - \xi)^3$ and the compression is $\eta = \Omega_0/\Omega$. The melt temperature T_m is given by the Lindemann expression [75]

$$T_m = T_{m0} e^{2a(1-1/\eta)} \eta^{2(\gamma_0 - a - 1/3)} \tag{61}$$

where T_{m0} is the melt temperature at ambient pressure, a is a constant, and γ_0 is the Grüneisen parameter at ambient pressure. We have parameterized the Grüneisen equation of state for the AlCu system [74]. All of the parameters have been calculated independent of the diffusivity simulations, so there are no free fitting parameters in $f(\Omega)$.

The results for the diffusivity using this pressure correction are much better than the simple forms gave, but the agreement with the MD results is less than ideal. The case of pure aluminum is shown in Fig. 13. We have taken the prefactor to be a fitting parameter, so the form (58) of the self-diffusivity is modified to be

$$D_H = \beta \left(\frac{\pi k_{\rm B} T}{M}\right)^{1/2} \left(\frac{6\Omega}{\pi \xi^2}\right)^{1/3} \frac{(1-\xi)^3}{\xi(1-\xi/2)} \tag{62}$$

In the fit the prefactor β was found to be 0.062 instead of 0.0206, so larger than the usual number by a factor of 3 [30]. Had we been interested in a narrower range of pressures near ambient, the fit would have been considerably better. As is, the MD diffusivity on the isotherms has a different functional dependence on the volume (or equivalently density or pressure) than the hard-sphere form (62). The MD results have less curvature as the volume changes than implied by the hard-sphere model. The qualitative trend of diffusivity increasing with temperature is described fairly well, but the quantitative level of agreement, while sufficient for many applications, is not entirely satisfactory.

We consider these results to be the best we can do in the context of a hard-sphere model. It is not surprising that the hard-sphere approximation breaks down at higher pressures and temperatures at which the classical turning point for the potential has been reduced considerably from its low-pressure, melt-temperature value. The accuracy of the hard-sphere model is not sufficiently good for our ultimate purposes in analyzing the MD simulations of the Kelvin-Helmholtz instability [19] mentioned in the introduction, so we are led to pursue other forms that are empirical but motivated by the hard sphere forms.

C. Empirical Model

The physics-based dilute gas and hard sphere models have not provided a satisfactory description of the MD results, so we consider an empirical form. We are motivated here by the form of the dilute hard sphere diffusivity, but modify the density dependence to be an affine variation and the temperature dependence to have a different exponent than the dilute hard sphere (exponent 0.5) and the dilute Lennard-Jones (exponent 1.65-2.0).

We are thus motivated to describe the MD results with a generalization of the dilute hard sphere diffusivity (55):

$$D_{AA^*} = d_0 + d_1 \left(\Omega - \Omega_0\right) \left(T/T_0\right)^n \tag{63}$$

where d_0, d_1, Ω_0 and n are parameters to be fit. For convenience, we have introduced a reference temperature T_0 taken to be 2000 K. It is not an independent parameter. The results for pure Al are better than the other models, as shown in Fig. 14. This model achieves the level of accuracy we want.

Based on the promising results with pure Al, we fit the entire set of MD results using the generalized dilute hard sphere formula (63), now taking the parameters d_0, d_1, Ω_0 and n to be quadratic functions of the mole fraction of copper, X. The values of the fit parameters are given in Table II. The results of the fit are shown in Figs. 15 and 16. The fits are good, with RMS errors of 6% and 12%, for Al and Cu self-diffusivities, respectively. The larger errors come from the super-cooled region.

Compared to the dilute hard sphere diffusivity (55), there are several notable differences and similarities. In both cases the diffusivity increases linearly with the volume per atom, but in the dilute hard sphere diffusivity it is strictly proportional to $\Omega \propto 1/\rho$, whereas in the generalization (63) there is a non-zero intercept. They are both power laws in the temperature, but for the dilute hard sphere the diffusivity is proportional to $\sqrt{T}$, whereas in the generalization it is almost linearly proportional to T: it goes like T^n with n ranging from 0.9967 to 1.12365 for Al and 0.963559 to 1.03212 for Cu.

The MD self-diffusivities fit to the generalized hard sphere diffusivity (63) with the parameters given in Table II are our principal results. The self-diffusivities can then be combined using the Darken equation (32) to determine the interdiffusivity, which is plotted in Fig. 17. The comparison of the Maxwell-Stefan diffusivity with the Darken diffusivity has shown that the contribution of cross-correlations is a small reduction in the diffusivity. We have made comparisons of the analytic model with the interdiffusivity computed from the rate of interface broadening in non-equilibrium MD simulations with an initially sharp interface between regions of pure Al and pure Cu [79]. The interdiffusivity from those simulations was a few percent larger than the analytic model predicts; i.e., the opposite direction from the change due to cross-correlations. Presumably, this increase in diffusivity results from activity corrections (the thermodynamic factor which we have not calculated).

VI. VISCOSITY

While the principal focus of this work is on diffusivity, we have also calculated the viscosity of molten AlCu mixtures. These calculations were done using the Green-Kubo integral of the shear stress autocorrelation function (9) for AlCu at temperatures ranging from 1000 K to 3000 K and pressures ranging from 0 to 25 GPa over a the range of copper concentrations 0–1. The autocorrelation function was calculated for each of the five independent components of shear stress and averaged. Whereas the velocity autocorrelation function was calculated on the fly as the simulations were running, the shear stress autocorrelation function was calculated by post-processing a file containing the stress components written at each time step. Finite size effects are much weaker for the viscosity than diffusivity, and negligible for the 4000 atom simulations.

The results are shown in Fig. 18. For example, the values of the viscosity for the pure metals at 2000 K and 4 GPa are $\eta_{\mathrm{Al}} = 0.00707$ poise and $\eta_{\mathrm{Cu}} = 0.0231$ poise (1 poise = 0.1 Pa-s). These correspond to kinematic viscosities of $\nu_{\mathrm{Al}} = 2.86 \times 10^{-7}$ m^2/s and $\nu_{\mathrm{Cu}} = 2.95 \times 10^{-7}$ m^2/s. The Schmidt number across the range of temperatures and densities calculated varies from 3.7 to over 2000 where

$$Sc = \frac{\eta}{\rho \mathscr{D}_{12}}. \tag{64}$$

The lower Schmidt numbers correspond to higher temperatures and lower pressures, and the highest numbers corresponding to supercooled liquids. There is some variation with concentration; e.g., at 2000 K and 4 GPa, the Schmidt number ranges from 13.5 to 33.8 as the concentration goes from 0 to 1.

The combination of the viscosity, diffusivity and radial distribution function results allow us to investigate whether the Stokes-Einstein relation holds. Taking the atomic radius $R = \frac{1}{2} r_{\mathrm{gmax}}$ (half the distance at the first peak of the radial distribution function), we have calculated the ratio

$$c_{\mathrm{SE}} = \frac{k_{\mathrm{B}} T}{\pi \, \eta \, D_i \, R} \tag{65}$$

for pure Al and pure Cu. For spherical particles, $c_{\mathrm{SE}} = 4$ for slip boundary conditions and 6 for no-slip. The results are shown in Fig. 65, where the behavior of the fluid is nearly that of the Stokes-Einstein relation with slip boundary conditions, except for those points in the supercooled region. The average value of c_{SE} is 4.24, slightly greater for aluminum than copper, and increasing slightly with volume and temperature. In the supercooled region the value of c_{SE} drops below 4.

We have fit an analytic expression to the viscosity values calculated from MD. The form of the expression is motivated by the Stokes-Einstein equation and the fact that the interatomic separation does not vary strongly over

the range of temperatures and pressures we have studied. The viscosity is fit to

$$\eta = \frac{k_{\rm B}T}{4\pi D_{\rm Cu}\, R(\Omega,T)} \tag{66}$$

$$R(\Omega,T) = (\Omega/V_{\rm Cu0})^{1/3}\, [R_{00} + R_1 \log(\Omega/V_{\rm Cu0})] \tag{67}$$

where $V_{\rm Cu0} = 11.7525\text{Å}^3$, the atomic volume of fcc copper at zero temperature and pressure. The expression for $D_{\rm Cu}$ is given by Eq. (63) with the values in Table II. In the Stokes-Einstein equation $R(\Omega,T)$ would be the radius of the atom, in particular the copper atom since we are using $D_{\rm Cu}$; however, we take it to be a fitting function of the form shown that is intended to capture variations in the atomic radius and $c_{\rm SE}$. The results of the best fit are given in Table III.

There have been more experimental studies of the viscosity of molten AlCu than of the diffusivity [12, 80–82]. To the best of our knowledge all of the work has been at ambient pressure. The most extensive viscosity study of copper-aluminum alloys was undertaken by Konstantinova et al. by measuring the viscous damping of torsional oscillations of the molten alloys in a crucible at high temperature [82]. They report kinematic viscosity, $\nu = \eta/\rho$, over a range of concentrations at temperatures of 600 °C to 1400 °C. At 700 °C (near our 1000 K results), they found that adding copper to aluminum increases the viscosity, in agreement with our results, but they found an anomaly at Al-25 at.% Cu (near the stoichiometric composition $CuAl_3$) where there is a peak in the viscosity. We do not see this peak, possibly because the peak is narrow and we have not calculated the viscosity at $X = 0.25$. A more interesting explanation is that there could be a propensity to form $CuAl_3$ clusters in molten AlCu due to some special property of the interatomic bonding that is not captured by the potential. Earlier experiments had not found this peak. The numerical values they report for kinematic viscosity at 700 °C range from 4.99×10^{-7} m^2/s^{-1} at $X = 0.0$ to 6.24×10^{-7} m^2/s^{-1} at $X = 0.4$ with the peak 8.48×10^{-7} m^2/s^{-1} at $X = 0.25$. The MD values for kinematic viscosity at 1000 K range from 3.64×10^{-7} m^2/s^{-1} at $X = 0.0$ to 4.40×10^{-7} m^2/s^{-1} at $X = 0.4$. The MD is systematically low compared to the experiment, but if the comparison is made at the same homologous temperature the values agree to $\sim 10\%$ apart from the peak due to the MD giving a low value for the melt temperature.

There have also been some experimental measurements of the viscosity of aluminum across a range of temperatures by Kononenko et al. [12]. They fit their data with the formula

$$\eta = 12.32 \times 10^{-8} \exp(1278/T) M\rho \tag{68}$$

with T in Kelvin, which gives $\eta = 11$ mP at $T = 933$ K [13]. This number is in reasonably good agreement with the MD result of 9 mP at $T = 1000$ K.

VII. THERMAL CONDUCTIVITY

The thermal conductivity has been calculated using Eq. (10). There are no electrons in our classical MD, so the electronic contribution to thermal conductivity is neglected. The thermal conductivity for pure Al is calculated to be 0.167 W/m·K at $T = 1964$ K and $p = 4.08$ GPa, and for pure Cu it is calculated to be 0.192 W/m·K at $T = 2000$ K and $p = 4.23$ GPa. Because electronic contributions dominate the thermal conductivity of the real molten metals, it is difficult to compare these numbers to experiment. For example, the thermal conductivity of pure molten aluminum at ambient pressure is reported to be in the range of 95–98 W/m·K at $T = 1000$ K based on experiment [76]. The thermal conductivity increases with temperature to 164 W/m·K at $T = 1900$ K according to quantum MD calculations [77]. This value is three orders of magnitude greater than the ionic contribution we have calculated. The thermal conductivity of copper is also dominated by electronic contributions, as typical for molten metals. The experimental results do not effectively constrain the value of the ionic contribution.

In order to make any comparison to a physical system, we need to consider a non-metallic liquid. As an example, the thermal conductivity of water ranges from 0.554 to 0.680 W/m·K as the temperature goes from 0 ° C to 200 ° C (it increases and then drops as the temperature is increased [78]). These values are somewhat larger than those we calculate for Al and Cu, but of the same order of magnitude.

VIII. CONCLUSION

We have used classical molecular dynamics to investigate the pressure and temperature dependence of diffusivity in molten AlCu mixtures over a broad range of conditions. The self-diffusivities were calculated using the Green-Kubo formula based on velocity autocorrelation function for the AlCu mixtures. Finite-size effects were addressed with a

hydrodynamic correction formula. Using the calculated self-diffusivities, we have assessed whether dilute hard sphere and dilute Lennard-Jones models apply to the molten mixture. Neither of the two dilute gas diffusivities describes the diffusivity in molten Al and Cu. We also considered a liquid hard-sphere model, extended to include a better description of the melt curve under pressure. This model is an improvement over the dilute gas models, but it too failed to reproduce the MD values sufficiently well. We have presented an empirical analytic form motivated by the dilute hard sphere diffusivity. This new form gives good agreement with the MD self-diffusivities across the range of temperatures (1000-3000 K) and pressures (0-25 GPa) simulated here. The agreement continues to be good up to the most extreme temperature (100000+ K) simulations.

The self-diffusivities have been combined using the Darken approximation to arrive at a model of interdiffusion across this range of thermodynamic conditions. The results have been compared with Maxwell-Stefan diffusivities to account for cross-correlation effects, which were found to make a small contribution to the diffusivity. The viscosities have been calculated from the shear stress autocorrelation function. An analytic form that reproduces the MD viscosity values has also been derived based on the Stokes-Einstein relation. The MD-derived transport coefficients have been found to be in good agreement with experimental data at ambient pressure. At higher pressures experimental data are not available, and the models make valuable predictions for transport under these extreme conditions. In the future it would be interesting to understand whether the functional forms used in the analytic models of self-diffusivity, interdiffusivity and viscosity reported here are in any sense universal. They may well apply to other molten metal alloys. It would be interesting to see whether they do, and if so, whether the form, currently empirical in nature, could be justified by further theoretical developments.

Acknowledgments

We acknowledge interesting discussions with A. W. Cook, J. N. Glosli, T. Haxhimali, E. R. Schwegler and D. A. White. We gratefully acknowledge support from the Laboratory Directed Research and Development (LDRD) program at Lawrence Livermore National Laboratory (LLNL) and supercomputer time provided through the Institutional Computing Grand Challenge program at LLNL. This work was performed under the auspices of the U.S. Department of Energy (DOE) by LLNL under Contract DE-AC52-07NA27344.

[1] K. K. Kuo, *Principles of Combustion* (Wiley-Interscience, New York, 1986).
[2] B. N. Kholodenko, Nat. Rev. Mol. Cell Biol. **7**, 165 (2006).
[3] R. R. Draxler, Atmos. Envir. **10**, 99 (1976).
[4] R. Jeanloz, Ann. Rev. Earth Planetary Sci. **18**, 357 (1990).
[5] J. W. Christian, *The Theory of Transformations in Metals and Alloys,* (Pergamon Press, Oxford, 2002).
[6] P. Amendt, O. L. Landen, H. F. Robey, C. K. Li and R. D. Petrasso, Phys. Rev. Lett. **105**, 115005 (2010).
[7] R. B. Bird, W. E. Stewart, and E. N. Lightfoot, *Transport Phenomena*, 2nd ed. (Wiley, New York, 2002).
[8] R. Hultgren, P. D. Desai, D. T. Hawkins, M. Gleiser, and K. K. Kelley, *Selected Values of the Thermodynamic Properties of Binary Alloys*, (American Society for Metals, Metals Park, OH, 1973).
[9] J. Henderson and L. Yang, Trans. Metall. Soc. AIME **221**, 72 (1961); L. Yang, S. Kado, and G. Derge, Trans. Metall. Soc. AIME **212**, 628 (1956).
[10] J. R. Wilson, Metall. Rev. **10**, 381 (1965).
[11] N. H. Nachtrieb, Adv. Phys. **16**, 309 (1967).
[12] V. I. Kononenko, S. P. Yatsenko, G. M. Rubinshtein, and I. M. Privalov, High Temp. (USA) **7**, 243 (1969).
[13] R. Bansal, J. Phys. C: Solid State Phys. **6**, 3071 (1973).
[14] A. K. Roy and R. P. Chhabra, Metall. Trans **19A**, 273 (1988).
[15] Y. Dua, Y. A. Chang, B. Huang, W. Gong, Z. Jin, H. Xua, Z. Yuan, Y. Liu, Y. Hea, and F.-Y. Xie, Mater. Sci. Engng. **A363** 140 (2003).
[16] U. Dahlborg, M. Besser, M. Calvo-Dahlborg, S. Janssen, F. Juranyi, M. J. Kramer, J. R. Morris, and D.J. Sordelet, J. Non-Cryst. Solids **353**, 3295 (2007).
[17] B. Zhang, A. Griesche, and A. Meyer, Phys. Rev. Lett. **104**, 035902 (2010).
[18] A. Meyer, Phys. Rev. B **81**, 012102 (2010).
[19] J.N. Glosli, K.J. Caspersen, D.F. Richards, R.E. Rudd, F.H. Streitz, and J.A. Gunnels, "Micron-scale Simulations of Kelvin-Helmholtz Instability with Atomistic Resolution," in Proc. ACM/IEEE SC07 Conference (Supercomputing 2007), Reno, NV, Nov. 2007, pp. 86–96.
[20] S. Chandrasekhar, *Hydrodynamic and Hydromagnetic Stability (International Series of Monographs on Physics)*, (Oxford Univ. Press, Oxford, 1961).

[21] S. Chapman and T. G. Cowling, *The Mathematical Theory of Non-uniform Gases* (Cambridge Univ. Press, Cambridge, 1952).
[22] J. H. Dymond, J. Chem. Phys. **60**, 969 (1974).
[23] M. E. Glicksman, *Diffusion in Solids: Field theory, solid-state principles and applications* (Wiley-Interscience, New York, 2000).
[24] P. Pechukas, Annu. Rev. Phys. Chem. **32**, 159 (1981).
[25] M. Dzugutov, Nature **381**, 137 (1996); see also the addendum Nature **411**, 720 (2001).
[26] Y. Rosenfeld, J. Phys.: Condens. Matter **11**, 5415-5427 (1999).
[27] S. Glasstone, K. J. Laidler, and H. Eyring, *Theory of Rate Processes*, (McGraw-Hill, New York, 1941).
[28] H. Eyring, D. Henderson, B. J. Stover, and E. M. Eyring, *Statistical Mechanics and Dynamics*, (Wiley, New York, 1964).
[29] Y. S. Badyal, U. Bafile, K. Miyazaki, I. M. de Schepper, and W. Montfrooij, Phys. Rev. E **68**, 061208 (2003).
[30] M. Shimoji, *Liquid Metals* (Academic Press, London, 1977).
[31] B. Alder and T. E. Wainwright, J. Chem. Phys. **33**, 1439 (1960).
[32] M. N. Rosenbluth and A. W. Rosenbluth, J. Chem. Phys. **22**, 881 (1954); W. W. Wood and J. D. Jacobson, J. Chem. Phys. **27**, 1207 (1957); A. Rotenberg, J. Chem. Phys. **42**, 1126 (1965).
[33] N. F. Carnahan and K. E. Starling, J. Chem. Phys. **51**, 635 (1969); *ibid* **53**, 600 (1969).
[34] J.-P. Hansen and I. R. McDonald, *Theory of Simple Liquids*, 2nd ed. (Academic Press, New York, 1986).
[35] P. Protopapas, H.C. Andersen, and N.A.D. Parlee, J. Chem. Phys. **59**, 15 (1973).
[36] J. Mei and J. W. Davenport, Phys. Rev. B **42**, 9682 (1990).
[37] D. Alfe and M. J. Gillan, Phys. Rev. Lett. **81**, 5161 (1998).
[38] L. Wang, X. Liu, Y. Zhang, Physica B **351**, 208 (2004).
[39] X. J. Han, M. Chen, and Y. J. Lu, Int. J. Thermophys. **29**, 1408 (2008).
[40] S. Yang, X. Su, J. Wang, F. Yin and N.-Y. Tang, Metall. Mater. Trans. A **40**, 3108 (2009).
[41] W. Götze, *Complex Dynamics of Glass-Forming Liquids: A Mode-Coupling Theory* (Oxford University Press, Oxford, UK, 2009).
[42] M. P. Allen and D. J. Tildesley, *Computer Simulation of Liquids* (Clarendon Press, Oxford, 1987).
[43] J. Trullàs and J. A. Padró, Phys. Rev. B **55**, 12210 (1997).
[44] S. Bastea, Phys. Rev. E **68**, 031204 (2003).
[45] J. Horbach, S. K. Das, A. Griesche, M.-P. Macht, G. Frohberg, and A. Meyer, Phys. Rev. B **75**, 174304 (2007).
[46] D. A. McQuarrie, *Statistical Mechanics* (Harper-Collins, New York, 1976).
[47] J. Trullàs and J. A. Padró, J. Chem. Phys. **99**, 3983 (1993).
[48] I. M. J. J. van de Ven-Lucassen, T. J. H. Vlugt, A. J. J. van der Zanden, and P. J. A. M. Kerkhof, Mol. Phys. **94**, 495 (1998).
[49] M. Schoen and C. Hoheisel, Mol. Phys. **52**, 33 (1984).
[50] E. J. Maginn, A. T. Bell, and D. N. Theodorou, J. Phys. Chem. **97**, 4173 (1993).
[51] L. S. Darken, Trans. AIME **175** 184 (1948).
[52] L. S. Darken and R. W. Gurry, *Physical Chemistry of Metals* (McGraw-Hill, New York, 1953), Ch. 18.
[53] J. R. Manning, Metall. Trans. **1** 499 (1970).
[54] S. Sridhar, Metall. Mater. Trans. **41B**, 275 (2010).
[55] G. A. Fernandez, J. Vrabec, and H. Hasse, Int. J. Thermophys. **25**, 175 (2004).
[56] R. E. Rudd and J. Q. Broughton, Phys. Stat. Sol. (b) **217**, 251 (2000).
[57] R. E. Rudd, Philos. Mag. **89**, 3133 (2009).
[58] R. E. Rudd, Mater. Sci. Forum **633-634**, 3 (2010).
[59] D. R. Mason, R. E. Rudd, and A. P. Sutton, Computer Physics Comm. **160**, 140 (2004).
[60] M. W. Finnis and J. E. Sinclair, Phil. Mag. A **50**, 45 (1984).
[61] D. R. Mason, R. E. Rudd, and A. P. Sutton, J. Phys.: Condens. Matter **16**, S2679 (2004).
[62] R. E. Rudd, D. R. Mason, and A. P. Sutton, Prog. Mater. Sci. **52**, 319 (2007).
[63] I. G. Brodova, P. S. Popel, and G. I. Eskin, *Liquid Metal Processing: Applications to Aluminium Alloy Production*, (Taylor and Francis, New York, 2002).
[64] For information on the *Zeus* and *Atlas* supercomputers see the internet site http://computing.llnl.gov.
[65] D. Nevins and F. Spera, Mol. Simul. **33**, 1261 (2007).
[66] B. Alder and T. E. Wainwright, Phys. Rev. A **1**, 18 (1970).
[67] I.-C. Yeh and G. Hummer, J. Phys. Chem. B **108**, 15873 (2004).
[68] M. D. Ediger, Annu. Rev. Phys. Chem. **51**, 99 (2000).
[69] F.J. Cherne and P.A. Deymier, Scripta Mater. **45**, 985 (2001).
[70] H. Mehrer, *Diffusion in Solids: Fundamentals, Methods, Materials, Diffusion-Controlled Processes*, 2nd ed. (Springer, Berlin, 2010), Ch. 8.
[71] T. E. Faber, *An Introduction to the Theory of Liquid Metals* (Cambridge Univ. Press, London, 1972).
[72] H. C. Longuet-Higgins and B. Widom, Mol. Phys. **8**, 549 (1964).
[73] P. Ascarelli, Phys. Rev. **173**, 271 (1968).
[74] R. E. Rudd, W. H. Cabot and K. J. Caspersen, "The Equation of State of Molten Alloys: a Classical Molecular Dynamics Study," Lawrence Livermore National Laboratory Report LLNL-JRNL-462918 (2010).
[75] D. J. Steinberg, S. G. Cochran, and M. W. Guinan, J. Appl. Phys. **51**, 1498 (1980).
[76] W.-K. Rhim and T. Ishikama, Rev. Sci. Instrum. **69**, 3628 (1998).

[77] V. Recoules and J.-P. Crocombette, Phys. Rev. B **72**, 104202 (2005).
[78] American Institute of Physics Handbook, D. E. Gray, ed. (McGraw-Hill, New York, 1957), pp. 4–70.
[79] K. J. Caspersen, W. H. Cabot, R. E. Rudd, and P. L. Miller, unpublished.
[80] S. Ganesan, R. Speiser, and D. R. Poirier, Metall. Trans. B **18**, 421 (1987).
[81] E. Gebhardt, M. Becher, and M. Doner, Aluminum **31**, 315 (1955).
[82] N. Yu. Konstantinova, P. S. Popel, and D. A. Yagodin, High Temp. **47**, 336 (2009).

Figures

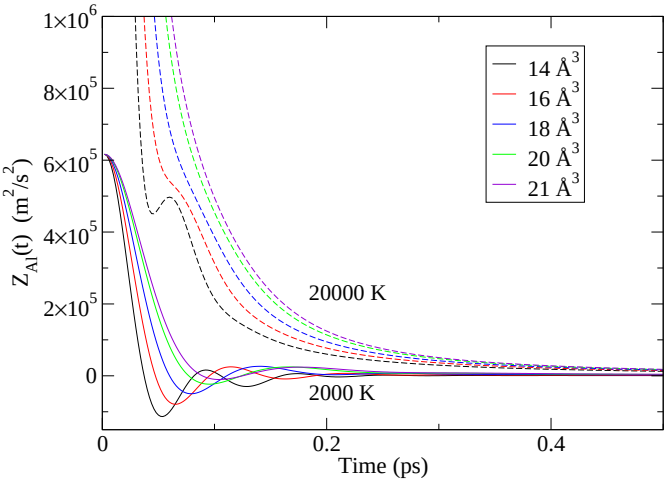

FIG. 1: (Color online) The velocity autocorrelation function for pure Al at the temperatures 2000 K (solid curves) and 20000 K (dashed curves). The curves correspond to the following volumes and pressures: 14 Å^3, 29 GPa (87 GPa); 16 Å^3, 14 GPa (60 GPa); 18 Å^3, 5.8 GPa (44 GPa); 20 Å^3, 1.4 GPa (33 GPa); and 21 Å^3, 0.12 GPa (29 GPa). The pressures at $T = 20000$ K are in parentheses. At the higher temperature much of the structure visible in the autocorrelation functions at 2000 K has disappeared except at 14 Å^3. The autocorrelation function was calculated out to a time of 1 ps (not shown).

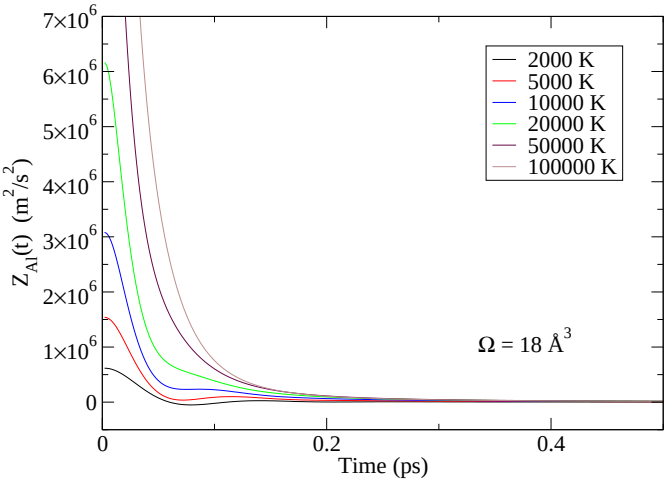

FIG. 2: (Color online) The velocity autocorrelation function for pure Al at various temperatures on the 18 Å^3 isochore. The curves correspond to the following temperatures and pressures: 2000 K, 5.8 GPa; 5000 K, 14 GPa; 10000 K, 26 GPa; 20000 K, 44 GPa; 50000 K, 87 GPa; and 100000 K, 150 GPa. The initial point of the curve $Z_{\rm Al}(0)$ increases linearly with the temperature. The autocorrelation function was calculated out to a time of 1 ps (not shown).

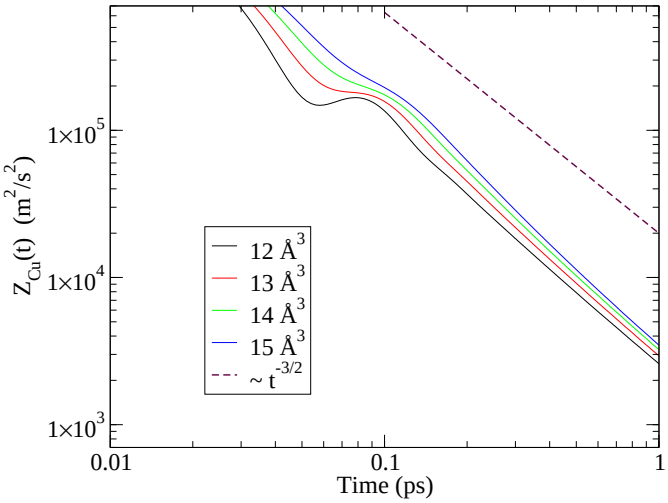

FIG. 3: (Color online) The diffusivity for pure Cu at the temperature 20000 K. The dashed line goes like $t^{-3/2}$, for comparison to show to what extent the long-time tails have that power-law dependence.

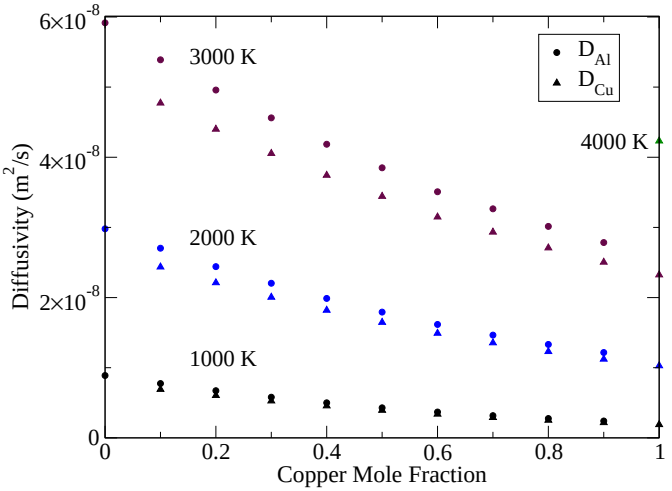

FIG. 4: (Color online) Self-diffusivity of Al and Cu in AlCu molten mixtures at ambient pressure and several temperatures: 1000 K, 2000 K and 3000 K (lower, middle and upper bands, respectively) as calculated by the Green-Kubo formula (8). One point at 4000 K is also shown.

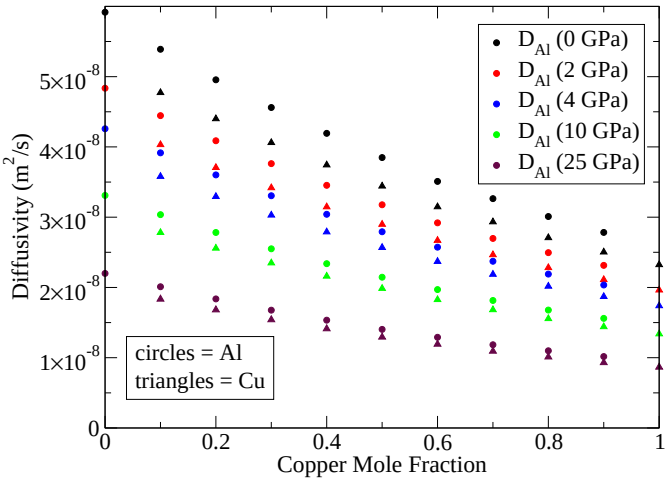

FIG. 5: (Color online) Self-diffusivity of Al and Cu in AlCu molten mixtures at a temperature of 3000 K and pressures ranging from 0 to 25 GPa. as calculated by the Green-Kubo formula (8). The diffusivity decreases with increasing pressure.

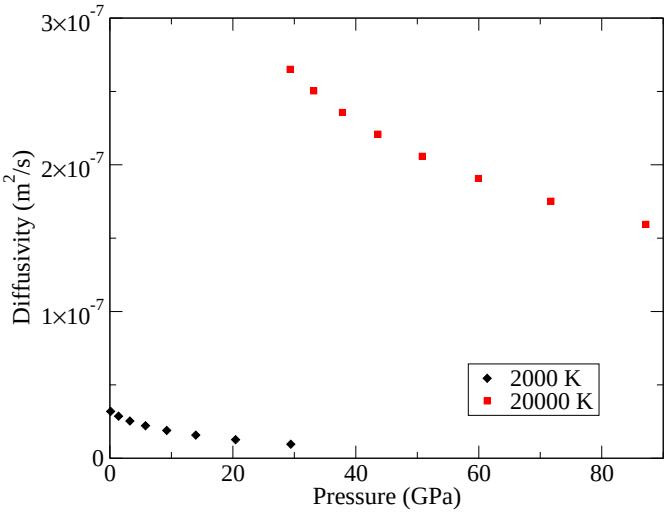

FIG. 6: (Color online) Self-diffusivity of Al in pure molten Al as a function of pressure at temperatures of 2000 K (diamonds) and 20000 K (squares). These diffusivity values have been calculated from the autocorrelation functions shown in Fig. 1 using the Green-Kubo formula (8). The points correspond to volumes per atom of 14, 15, . . . , 21 Å^3.

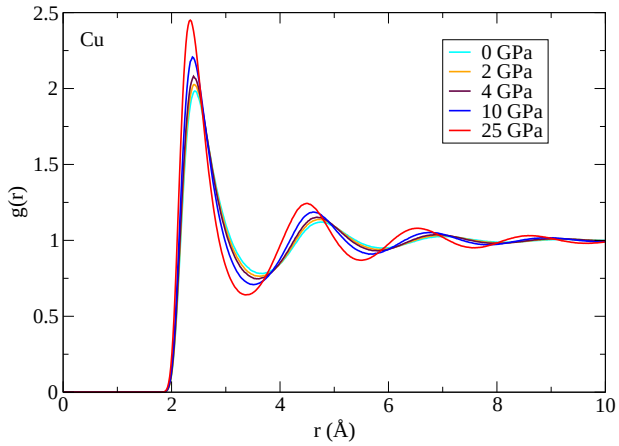

FIG. 7: (Color online) The radial distribution function $g(r)$ for Cu at a temperature of 3000 K, as calculated by MD.

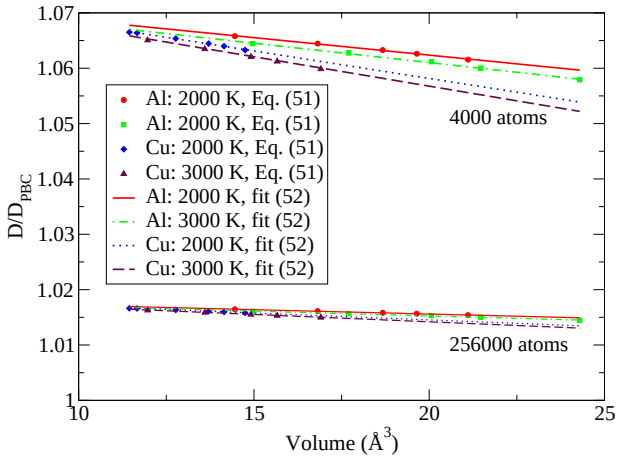

FIG. 8: (Color online) The multiplicative correction due to finite size effects with periodic boundary conditions as a function of atomic volume, Ω. The points are the correction obtained from Eq. (51) using the values for the nearest neighbor separation a given in Table I. The curves are the fits from Eq. (52).

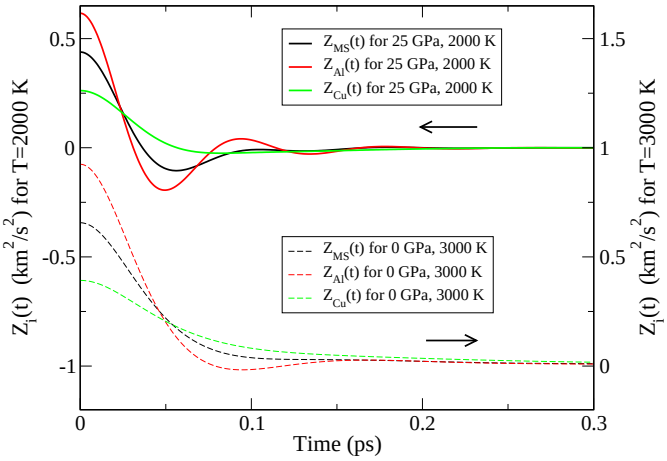

FIG. 9: (Color online) The velocity autocorrelation functions for X=0.5 AlCu at $p = 25$ GPa and $T = 2000$ K (solid curves) and $p = 0$ GPa and $T = 3000$ K (dashed curves). The y-axis has been offset to separate the two sets of curves, with the arrows indicating which vertical axis goes with which curves: 2000 K on the left and 3000 K on the right. The correlations functions for the Maxwell-Stefan diffusivity $Z_{\rm MS}(t)$ (28) and the self-diffusivities $Z_{\rm Al}(t)$ and $Z_{\rm Cu}(t)$ (16) are shown for comparison. The autocorrelation functions were calculated out to a time of 1 ps (not shown).

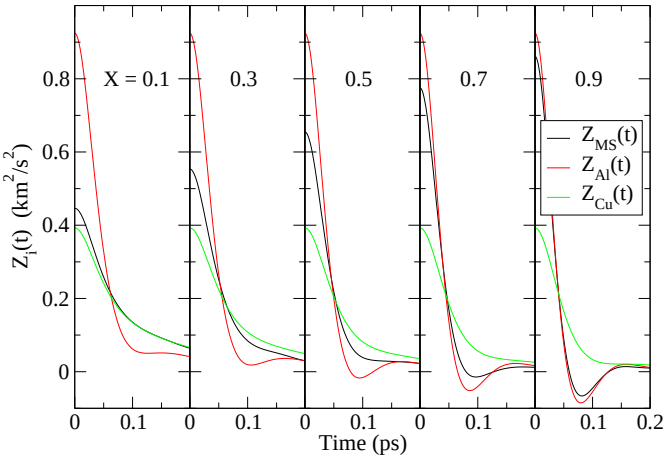

FIG. 10: (Color online) The velocity autocorrelation functions for AlCu mixtures at a pressure of 0 GPa and the temperatures 3000 K. The mole fractions range from 0.1 to 0.9, as indicated in the 5 panels. The correlations functions for the Maxwell-Stefan diffusivity $Z_{\rm MS}(t)$ (28) and the self-diffusivities $Z_{\rm Al}(t)$ and $Z_{\rm Cu}(t)$ (16) are shown for comparison. As the concentration is changed, $Z_{\rm MS}(t)$ varies from nearly equal to $Z_{\rm Cu}(t)$ at $X = 0.1$ to nearly equal to $Z_{\rm Al}(t)$ at X=0.9.

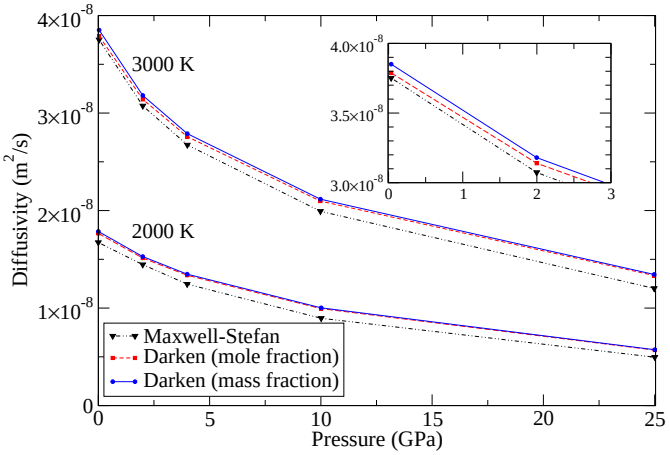

FIG. 11: (Color online) Diffusivity plotted as a function of pressure. The diffusivities plotted are the Maxwell-Stefan diffusivity $Đ_{12}$ and the corresponding diffusivities derived from the Darken relations based on mole fraction weighting (31) and mass fraction weighting (44) of the self-diffusivities. The plotted values are for $X = 0.5$ and the temperatures indicated: 2000 K and 3000 K. The inset shows the 3000 K curves at low pressure where the mole fraction weighting gives a significantly better approximation to $Đ_{12}$.

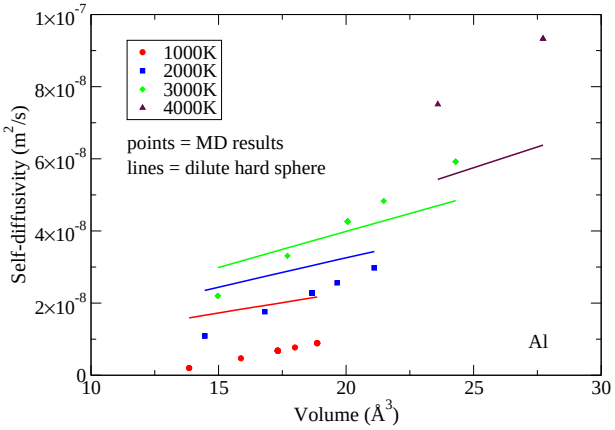

FIG. 12: (Color online) Self-diffusivity (tracer diffusivity) of Al pure molten Al at four temperatures: 1000 K, 2000 K, 3000 K and 4000 K. The points are values as calculated with MD using the Green-Kubo formula (8). The lines are fit using the dilute hard sphere formula (55) with $d = 2.4$Å. The dilute hard sphere model does not provide a highly accurate description of the diffusivity.

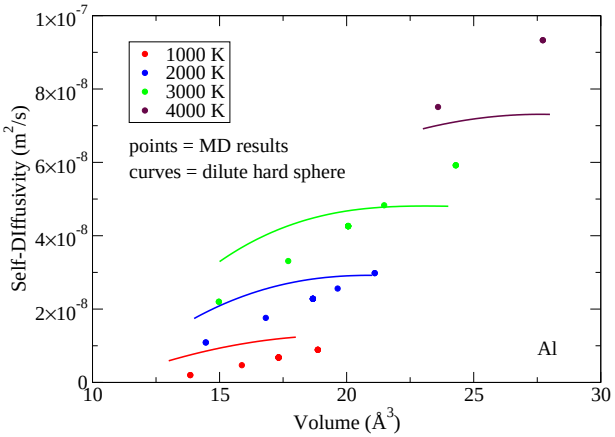

FIG. 13: (Color online) Self-diffusivity (tracer diffusivity) of Al pure molten Al at four temperatures: 1000 K, 2000 K, 3000 K and 4000 K. The points are values calculated with MD using the Green-Kubo formula (8). The curves are fit to the dense hard sphere formula (62). The dense hard sphere model is an improvement over the dilute model shown in Fig. 12, but it still is not as accurate as desired.

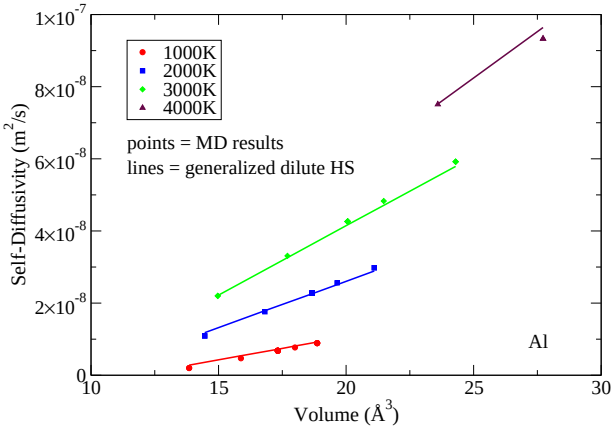

FIG. 14: (Color online) Self-diffusivity (tracer diffusivity) of Al pure molten Al at four temperatures: 1000 K, 2000 K, 3000 K and 4000 K. The points are values calculated with MD using the Green-Kubo formula (8). The curves are fit to the generalized dilute hard sphere formula (63). This empirical fit is an improvement over the other models.

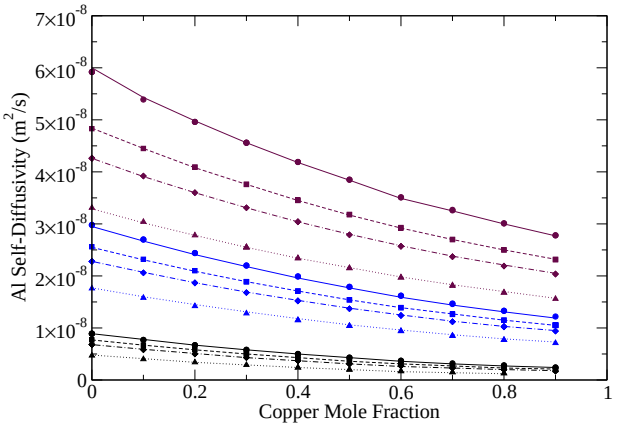

FIG. 15: (Color online) Self-diffusivity (tracer diffusivity) of Al as a function of copper fraction. The points are values calculated with MD using the Green-Kubo formula (8). The curves are fit to the generalized dilute hard sphere formula (63). The upper band of four curves is at 3000 K; the middle band of four curves is at 2000 K; the lower band of four curves is at 1000 K. The circular points and solid curves represent 0 GPa; square points and dashed curves, 2 GPa; diamond points and dot-dashed curves, 4 GPa; triangular points and dotted curves, 10 GPa. The curves and points end at a mole fraction of 0.9 since the Al self-diffusivity is not defined at the next point (a pure Cu system).

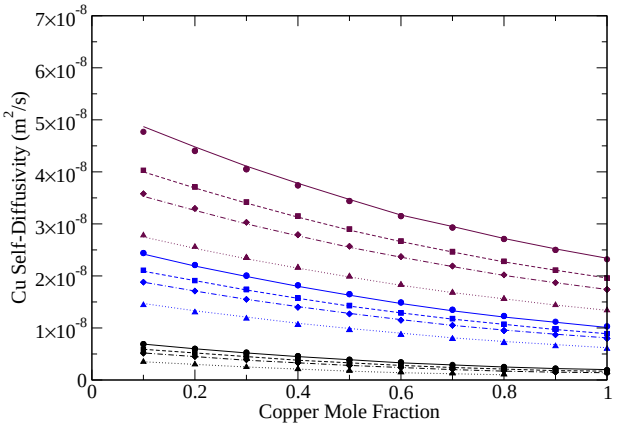

FIG. 16: (Color online) Self-diffusivity (tracer diffusivity) of Cu as a function of copper fraction, as in Fig. 15 except for Cu instead of Al.

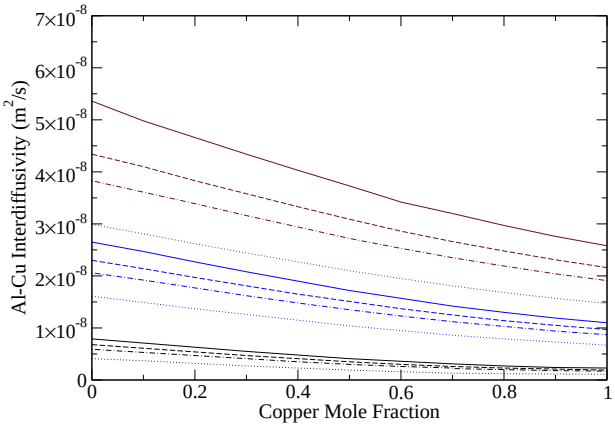

FIG. 17: (Color online) AlCu interdiffusivity calculated in MD from the self-diffusivity (63) and combined according to the generalized Darken equation (44). The line color and style follow the same pattern as in Fig. 15.

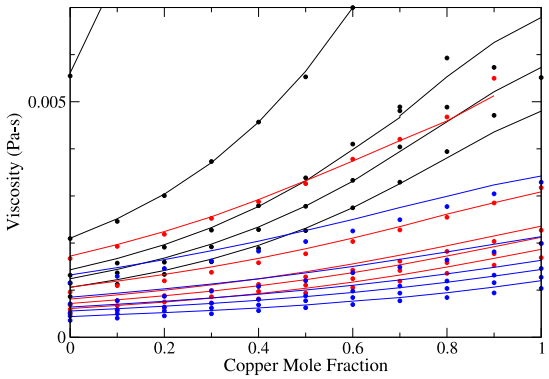

FIG. 18: (Color online) The viscosity as a function of concentration across a range of pressures and temperature. The solid curves show the fit to Eq. 67 and the points show the results of the MD simulations.

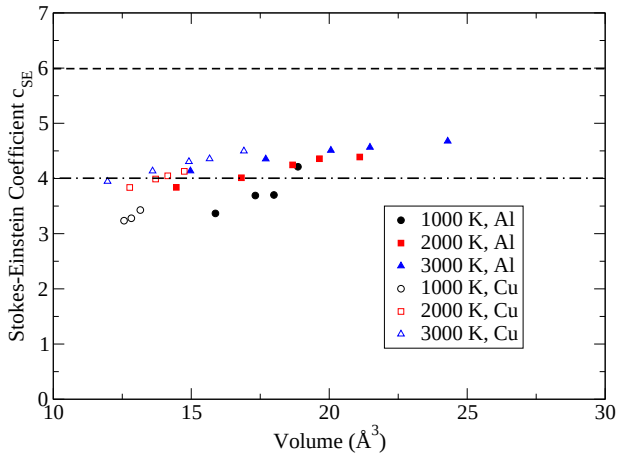

FIG. 19: (Color online) The Stokes-Einstein coefficient (65). In the Stokes-Einstein relation this number would be 4 for slip boundary conditions (dot-dash line) and 6 for no-slip (dashed line).

Tables

TABLE I: Nearest neighbor separation calculated from the first peak in the radial distribution function $g(r)$.

Pressure	a_{Al}(2000 K)	a_{Al}(3000 K)	a_{Cu}(2000 K)	a_{Cu}(3000 K)
0 GPa	2.690 Å	2.661 Å	2.450 Å	2.433 Å
2 GPa	2.669 Å	2.642 Å	2.441 Å	2.423 Å
4 GPa	2.650 Å	2.629 Å	2.432 Å	2.414 Å
10 GPa	2.604 Å	2.583 Å	2.407 Å	2.391 Å
25 GPa	2.524 Å	2.504 Å	2.359 Å	2.345 Å

TABLE II: Parameters for the generalized hard sphere diffusivity (63) fit to the MD self-diffusivities as a function of the mole fraction of copper, X.

Species	d_0 (10^{-9} m^2/s)	d_1 (10^{-9} m^2/s·Å^3)	Ω_0 (Å^3)	n
Al	$-5.574 + 1.810X + 1.549X^2$	$2.742 - 0.6729X + 0.06810X^2$	$8.329 - 0.1079X + 0.3641X^2$	$0.9967 + 0.004351X + 0.1226X^2$
Cu	$-6.021 + 2.068X + 1.177X^2$	$2.432 - 0.4977X + 0.06156X^2$	$7.725 + 0.1270X + 0.4212X^2$	$0.9646 - 0.01898X + 0.0865X^2$

TABLE III: Parameters for the analytic expression for viscosity (67). The parameters are functions of the mole fraction of copper, X, as indicated.

R_0 (Å)	$1.09784 - 0.422212X + 0.401049X^2$
R_1 (Å)	$0.312254 + 0.74701X + 0.334005X^2 - 1.31185X^3$